



Effects of elevated temperature and water re-curing on the compression behavior of hybrid fiber reinforced concrete

Fengzhen He^{a,b}, Luigi Biolzi^b, Valter Carvelli^{b,*}

^a School of Mines, China University of Mining and Technology, Xuzhou, 221116, China

^b Department A.B.C., Politecnico di Milano, Piazza Leonardo Da Vinci 32, 20133, Milan, Italy

ARTICLE INFO

Keywords:

Concrete
Hybrid fibers
Elevated temperature
Water re-curing
Compression behavior

ABSTRACT

Over the past decades, the effect of elevated temperatures on the mechanical properties of concrete has received significant attention because of the importance for fireproof design, safety evaluation and repair of fire damaged constructions. However, very few researches have been dedicated to the consequences of water re-curing of a thermally damaged concrete. In this paper, the effect of elevated temperatures and water re-curing on the mechanical response of two hybrid fiber reinforced concretes was investigated. For the first hybrid reinforced mix, long hooked-end and medium hooked-end steel fibers were adopted, as well as high strength short wave shaped steel fibers. In the second mix, polypropylene fibers substituted the short-wave shaped steel fibers. The mechanical behavior in compression was studied by measuring the stress-strain response. The elevated temperatures above 200 °C decreased: Young's modulus, compressive strength and toughness of the hybrid fiber reinforced concretes. The stable crack growth stage was reduced with the increase of the temperature above 200 °C, with an extension of the unstable crack growth stage for both kinds of hybrid fiber reinforced concrete. Water re-curing partially recovered Young's modulus, compressive strength, toughness, and extended the stable crack growth. An existing model was modified for predicting the stress-strain response of thermally damaged hybrid fiber reinforced concrete.

1. Introduction

Fire is one of the most serious potential risks to most of the constructions [1]. Concrete structures are likely to experience thermal damage by accidental causes or by special application purposes [2]. When exposed to high temperatures, the dense micro-structure inhibits the evaporation of physical and chemical water, leading to high vapor pressure in concrete [1,3]. The low thermal conductivity of concrete [4,5] creates a thermal gradient, from the surface to the center of the concrete, and a considerable thermal stress state with compressive component parallel to the heated surface [6], and tensile one in the direction perpendicular to the heated surface. The vapor pressure and thermal stress motivate the onset and propagation of both micro- and macro-cracks, leading to the spalling of concrete. When the temperature exceeds a certain level [7,8], the decomposition of the matrix and aggregates leads to a serious reduction in the load-carrying capacity of concrete.

Fibers reinforcement can not only reduce the brittleness of concrete but also improve fire resistance [1,3,9,10]. The presence of polypropylene fibers has a negligible effect on concrete compressive strength, but it can reduce or eliminate the spalling when exposed to high temperature [9,11–15]. It is attributed to the low melting point of the polypropylene fiber. Steel fibers, with higher elastic

* Corresponding author.

E-mail address: valter.carvelli@polimi.it (V. Carvelli).

modulus, improve the mechanical performance of concrete by bridging cracks [16–19]. But, the effect of the steel fiber on concrete exposed to high temperatures is controversial [1,2,20–22]. The presence of the steel fibers restricts the propagation of cracks and increases the heat transfer ability. But steel fibers produce extra voids and micro cracks, increasing the chance for the propagation of micro cracks under high temperature.

There is a general agreement on the favorable influence of fiber hybridization on the mechanical performance of fiber reinforced concrete [1]. Studies [1,13,23] indicate better performance of the hybrid fiber reinforced concrete at elevated temperature. But investigations on the hybrid steel fiber under high temperature are limited. The influence of the hybridization type on the compression performance of the thermally damaged hybrid fiber reinforced concrete is not clear. Therefore, it worth conducting more in-depth research on the compression behavior of the hybrid fiber reinforced concrete exposed to elevated temperature.

Under high temperature, the compositions of the concrete experience chemical and physical change, leading to the change of the micro structure of the cement matrix [24]. The deterioration of micro structure of concrete due to high temperatures produces a significant effect on the failure mechanisms, which is directly reflected by the compression stress-strain curves [25]. A large number of researchers [15,23,25–28] investigated the plain concrete compressive performance according to the stress-axial strain behavior, providing essential information for the safety maintenance of concrete structures. But, the thermal mechanical change of concrete can not be reflected comprehensively only by the stress-axial strain. A more complex scenario is for fiber reinforced concrete. The randomly distributed fibers provide constraining effect in both axial and transverse directions, producing a more considerable effect on the volumetric strain than the axial one [2,29–31]. Existing fire design codes [32–34] are based on plain concrete. Extrapolation of the guidelines to hybrid fiber reinforced concrete may not be appropriate.

Restoring the fire-damaged concrete structure to the safety level by adopting the proper post-fire re-curing methods is a sustainable way for reducing the consumption of concrete. During the post-fire stage, the dehydrated compounds react with the water and carbon dioxide (CO_2), producing some composites filling the cracks and voids in the cement matrix. These newly generated composites can produce positive [35,36] or negative [37–39] effects on the post-heating mechanical behavior. The negative effects can be attenuated by proper post re-curing, which can help to recover the mechanical behavior of the thermally damaged concrete. Water re-curing is one post-fire strategy proposed to reactivate chemical reactions. However, water re-curing is debatable [35,36,40–42]. The influence of the water re-curing on the compressive performance of thermally damaged hybrid fiber reinforced concrete has not investigated in detail.

In this study, the effect of hybridization of fibers, high temperature, and water re-curing on the compressive performance of hybrid fiber reinforced concrete was investigated by conducting uniaxial compression tests on cylindrical specimens. Water evaporation, damage degree, damage initiation stress, and critical stress of the thermally damaged hybrid fiber reinforced concrete were analyzed. The water re-curing effect on the performance of the thermally damaged hybrid fire reinforced concrete was evaluated. An available model was adopted for the prediction of the compressive strength-strain relationship.

2. Materials and methods

2.1. Materials

Portland Cement CEM II/A-LL42.5R, river gravel with the maximum nominal size of 16 mm, and crushed limestone with the maximum nominal size of 22 mm were used. The fine aggregate was river sand having a maximum size of 4 mm. The grading curves of aggregates are shown in Fig. 1. The additive Aeternum Proof [43] was used to keep good workability. The specimens were produced in a precast plant under a strict quality control to guarantee the uniformity of the batches performance [44].

Four kinds of commercial fibers with different geometric parameters and materials were selected according to a preliminary study [45] on fibers available in the market. The high strength short steel fiber has a waved shape, while the long and medium fibers has hooked-ends. The polypropylene fiber has a melting point of 170 °C, and therefore are not suitable for concrete reinforcement exposed

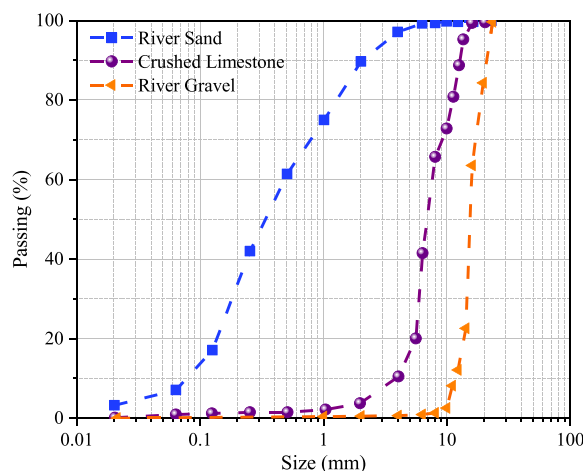


Fig. 1. Grading curves of the aggregates.

to elevated temperatures. The main motivation for exploiting polypropylene fibers as reinforcement, also mentioned in the literature (see e.g. Refs. [6,9,11,12]), is the extra paths for the evaporation of the water created by the melting of the fibers, which can reduce the vapor pressure and, then, damage in concrete. The properties of the fibers are listed in Table 1.

2.2. Mixing design and specimen casting

Two concrete mixtures were designed, as shown in Table 2. The components, except fibers, were the same. Mix named 'S' embedded long hooked-end steel fiber (LS), medium hooked-end steel fiber (MS), and short wave-shaped steel fiber (SS). In the mix named 'P', the short wave-shaped steel fibers were replaced by the polypropylene fibers (PP). The volume fractions of fibers in both mix groups were the same. The specimens were cast according to the European standard EN 12390-2:2019 [46]. The specimens were kept in the molds for 24 h. Then, they were demolded and cured in a chamber with a temperature of $20 \pm 2^\circ\text{C}$ and relative humidity of $90 \pm 3\%$ until testing.

2.3. Testing methods

The compressive performance of hybrid fiber reinforced concrete under different pre-conditionings, as shown in Table 3, was studied by the uniaxial compression test on cylinders with the dimensions Diameter \times Height = 100 mm \times 200 mm according to the European standard EN 12390-3:2019 [47]. For each condition, three or more specimens were tested. It must be highlighted that the size effect dependency of the reinforced concrete mechanical properties was not considered. It can be topic of further study. The testing ID includes fiber type, temperature, and post-heating re-curing condition. For example, PW-400 represents mix with short polypropylene fibers, 400 $^\circ\text{C}$ heating, and water re-curing after heating. Before the compression test, the specimens were heated to the target temperature (200 $^\circ\text{C}$, 400 $^\circ\text{C}$, 600 $^\circ\text{C}$, 800 $^\circ\text{C}$) with the rate of 1 $^\circ\text{C}/\text{min}$. Then, the target temperature was kept constant in the furnace for 2 h, before cooling to ambient temperature with the rate of 1 $^\circ\text{C}/\text{min}$. The specimens exposed to 400 $^\circ\text{C}$ and 600 $^\circ\text{C}$ were post-cured in water for three weeks [35,48], then were taken out and cured in the lab environment for one week.

The setup of the compression test is shown in Fig. 2. Three linear variable displacement transducers (LVDT), positioned at 120 $^\circ$ each other, were used to measure the axial strain. To reduce the end constraint effect, the LVDTs were located 50 mm far from the ends. Teflon film was used to reduce the friction caused by the loading plates. The lateral strain was monitored by the clip gauge. The test was started by the LVDT control with a rate of 0.0015 mm/s. The clip gauge control with a rate of 0.001 mm/s was activated when the lateral displacement reached 0.020 mm. The test was stopped when the lateral displacement was 3.5 mm, the maximum of the clip gauge.

For each pre-conditioning, the ultrasonic pulse velocity (UPV) in the longitudinal direction of the cylinder specimen was measured before and after heating or water re-curing for evaluating the damage degree of hybrid fiber reinforced concrete exposed to high temperature. The measurement was conducted according to the European standard EN 12504-4:202 [49]. Moreover, the water evaporation after the high temperature exposition was measured by weighting the mass of the specimens before and after heating or water re-curing.

3. Water evaporation analysis

Capillary water, inter-layer water, and chemical combined water are the three kinds of water in concrete [35,50–52]. Under the high temperature environment, water evaporates from inside to the outside, leading to physical (pore and microstructure) and chemical changes (dehydration of the C–S–H). Meanwhile, water evaporation produces high vapor pressure, accelerating the propagation of the cracks in concrete. Therefore, the water evaporation ratio can reflect the micro structure and mechanical property change to a certain extent.

Fig. 3 shows the water evaporation ratio of hybrid fiber reinforced concrete under different testing scenarios. Both kinds of hybrid fiber reinforced concrete had an almost bi-linearly increase of water evaporation with temperature Fig. 3(a). The average water evaporation ratio at 400 $^\circ\text{C}$ reached 8.30% and 6.78% for Mix P and Mix S, accounting for 67.8% and 59.5% of that at 800 $^\circ\text{C}$. Capillary water evaporated easily when the temperature increased from 20 $^\circ\text{C}$ to 400 $^\circ\text{C}$. The inter-layer water between the layers of the C–S–H [52,53] evaporated when the temperature exceeded 200 $^\circ\text{C}$. Some composites, like calcium hydroxide and aggregates, experienced decomposition and the chemical water in them evaporated, leading to the further increase of the water evaporation. The melting and evaporation of the polypropylene fiber when the temperature exceeded 170 $^\circ\text{C}$ provided extra paths for water evaporation, leading to

Table 1
Properties of fibers.

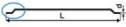
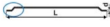


	Long (L) hooked-end	Medium (M) hooked-end	Short (S) wave-shaped	Polypropylene (PP)
				
Length (mm)	50	35	18	18
Diameter (mm)	1.0	0.6	0.2	0.01
Aspect ratio (L/D)	50	58	90	1800
Density (kg/m ³)	7800	7800	7800	910
Tensile Strength (N/mm ²)	1440	1250	2600	450
Modulus of elasticity (GPa)	200	200	200	37

Table 2
Concrete mixtures.

Mix group	W/C	Cement (kg/m ³)	Aggregates(kg/m ³)			Volume fraction of fiber (%)				Additive (kg/m ³)
			River gravel	Crushed limestone	River sand	LS	MS	SS	PP	
S	0.45	450	705	530	320	0.65	0.65	0.2	–	13.5
P			705	530	320	0.65	0.65	–	0.2	13.5

Table 3
Testing groups.

ID	Temperature (°C)	Water re-curing	ID	Temperature (°C)	Water re-curing
S-20	20	NO	PW-400	400	YES
P-20	20	NO	P-600	600	NO
S-200	200	NO	S-600	600	NO
P-200	200	NO	SW-600	600	YES
S-400	400	NO	P-800	800	NO
SW-400	400	YES	S-800	800	NO
P-400	400	NO			

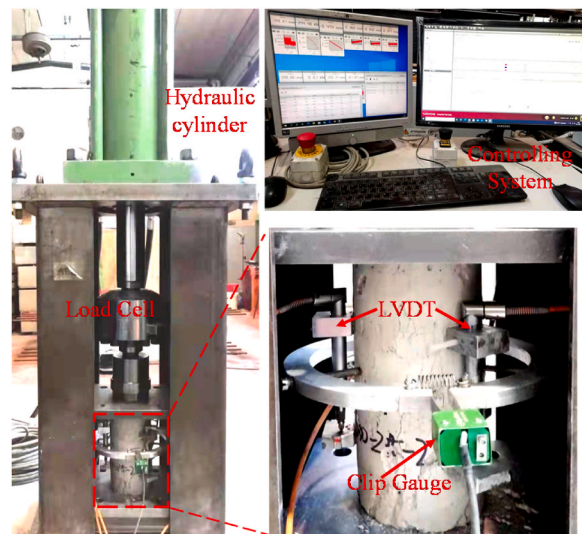


Fig. 2. Experimental setup for compression test.

the higher water evaporation ratio in Mix P than that of Mix S.

Water re-curing decreased the water evaporation as shown in Fig. 3(b). The water evaporation ratios of Mix S and Mix P decreased from 8.17% and 7.69% to 0.28% and 0.30%, respectively, which were similar to that at 600 °C. During the water re-curing period, the decomposed composites underwent the rehydration process, producing C–S–H, Ca(OH)₂, CaCO₃, and others [36,54]. Moreover, free water filled the voids, cracks and capillary pores.

4. Damage degree

The non-destructive ultrasonic pulse velocity (UPV) method, a preferred non-destructive method for damage evaluation in civil engineering [55–59], was adopted to evaluate the deterioration of concrete caused by high temperature. The UPV in the longitudinal direction of the cylinder was measured before and after high temperature exposition and water re-curing. The Damage Degree (DD) [57], according to the variation of UPV, was adopted to evaluate the deterioration of the hybrid fiber reinforced concrete:

$$DD = 1 - \frac{V}{V_0} \quad (1)$$

where V is the ultrasonic pulse velocity after the temperature exposition or water re-curing, V₀ is the UPV of the cylindrical specimen at 20 °C. The higher damage degree indicated the more serious damage.

The damage degree increased with temperature for both kinds of hybrid fiber reinforced concrete as shown in Fig. 4(a). The lower deterioration was recorded for temperature below 200 °C as the damage degree was about 0.1. The evaporation of the capillary water

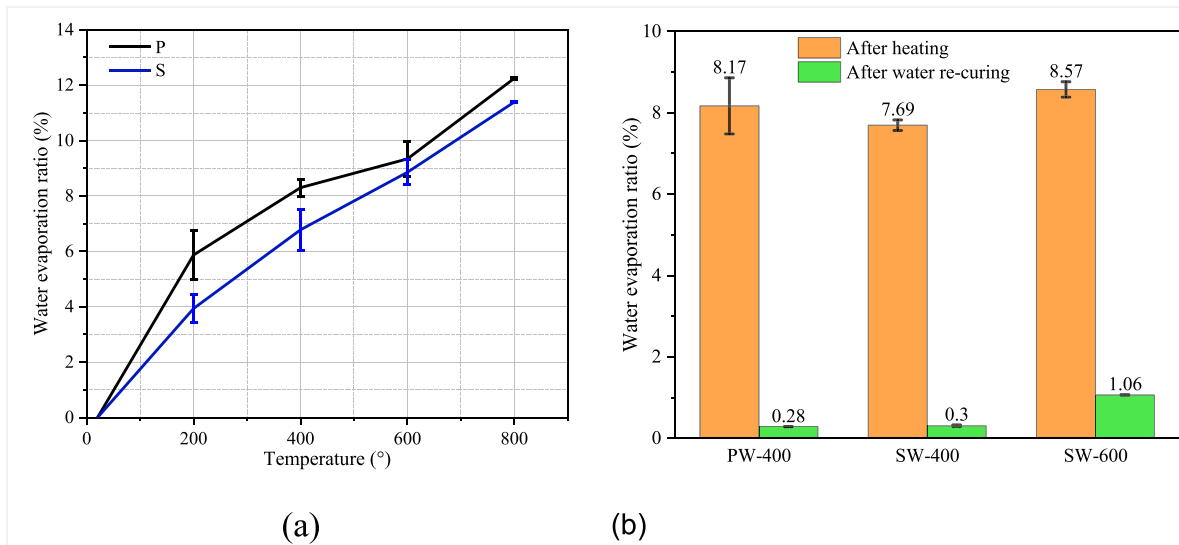


Fig. 3. Water evaporation ratio: (a) after heating and (b) after heating and water re-curing. Error bars show the standard deviation of 3 replicas.

was the main reason for the increase of the damage degree. Under heating, the capillary water (free water) flowed from the heated surface into the inner part of the concrete with low vapor pressure. The steam condensed in the inner region with a temperature around 100 °C, forming a saturated layer. The saturated layer, like moisture clog wall, blocked the evaporation of the water, increasing the pore pressure in concrete [60,61]. The damage degree rose up to about 0.65 when the temperature increased from 200 °C to 600 °C. Exceeding 200 °C, the C–S–H micro structure experienced decomposition, leading to the generation of cracks in the matrix. Meanwhile, the mismatch of the thermal expansion between aggregates and cement paste produced micro cracks in the Interface Transition Zone (ITZ) [62]. For exposition to temperature higher than 600 °C, the decomposition of the aggregates, calcium hydroxide ($\text{Ca}(\text{OH})_2$), and carbonates happened [63], causing considerable damage in concrete, leading to further growth of the damage degree, more than 0.7 at 800 °C. When the temperature increased from 400 °C to 600 °C, large cracks surrounded by several small cracks appeared on the surface of the specimens. It proved the deterioration of the internal structure of the concrete with the increase of the temperature.

Water re-curing reduced the damage degree for both kinds of thermally damage hybrid fiber reinforced concrete as shown in Fig. 4 (b). The average damage degree of Mix S decreased from 0.39 to 0.63 to 0.07 and 0.10 at 400 °C and 600 °C, respectively. During the water re-curing period, the rehydration of the decomposed phrases produced compositions, like C–S–H and CaCO_3 , bridging the cracks in concrete. The crack patterns, as shown in Fig. 5 (surface portion where damage was more visible by naked eye), provided evidence for

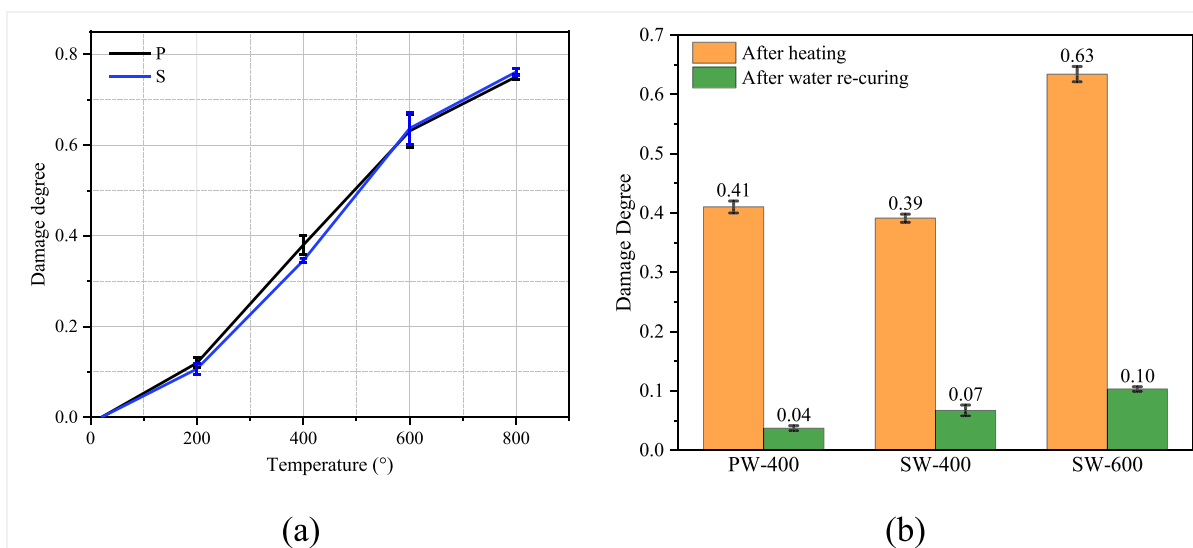


Fig. 4. Damage degree after: (a) high temperature exposition and (b) high temperature exposition and water re-curing. Error bars show the standard deviation of 3 replicas.

the repairing effect of the water re-curing on the thermally damaged hybrid fiber reinforced concrete. Only some small cracks were detected after water re-curing. Free water refilled the voids and cracks. These resulted in a positive effect as measured by the ultrasonic pulse wave propagation.

5. Compression behavior

5.1. Compressive strength and peak strain

Fig. 6 compares the compressive strength of both thermally damaged hybrid fiber reinforced concretes. The compressive strength decreased with temperature. For Mix S, the elevated temperature below 200 °C had a negligible effect on the compressive strength, staying close to 56.2 MPa. A considerable reduction was measured when the temperature exceeded 200 °C, and especially when the temperature exceeded 400 °C. The compressive strength decreased by 87%, reaching 7.16 MPa at 800 °C. It was consequence of the increase of internal vapor pressure and thermal stress with high temperature, leading to the generation and extension of cracks in the ITZ and cement matrix [1,62]. Moreover, the C–S–H started the decomposition process when the temperature exceeded 100 °C, while $\text{Ca}(\text{OH})_2$ and carbonates dehydrated when the temperature reached 450 °C and 700 °C, respectively [61]. These changes weakened micro structures of matrix, reducing the load-bearing capacity. Mix P had a similar trend to Mix S. But the compressive strength of mix S was higher than that of mix P. The short wave-shaped steel fiber had higher bonding strength, generating a more effective bridging effect on the propagation of micro cracks. The polypropylene fibers melted and evaporated when the temperature exceeded 170 °C, losing the bridging effect.

Water re-curing partially recovered the compressive strength for both thermally damaged hybrid fiber reinforced concretes as shown in Fig. 6(a). For Mix S, at 400 °C, the compressive strength remained 80% of the compressive strength at 20 °C, indicating that damage on bonding between steel fibers and the cement matrix and ITZ was not serious. Therefore, rehydration compositions had a negligible effect on the recovery of compressive strength. At 600 °C, the cracks caused by the high temperature were intensive. The rehydration bridged or narrowed the cracks, leading to the recovery of the strength of matrix. For Mix P, the water re-curing was more effective. The compressive strength increased from 20.59 MPa to 31.60 MPa at 400 °C. It was because the rehydrated productions filled the cracks and voids caused by the evaporation of the polypropylene fibers.

The relationship between temperature and nominal residual compressive strength (defined as the ratio between compressive strength of the thermally damaged concrete f_{CT} and compressive strength at 20 °C f_{C20}) was detected in the range from 20 °C to 800 °C, as shown in Fig. 6(b). The fitting functions of the experimental data are given by Eqn. (2) and Eqn. (3).

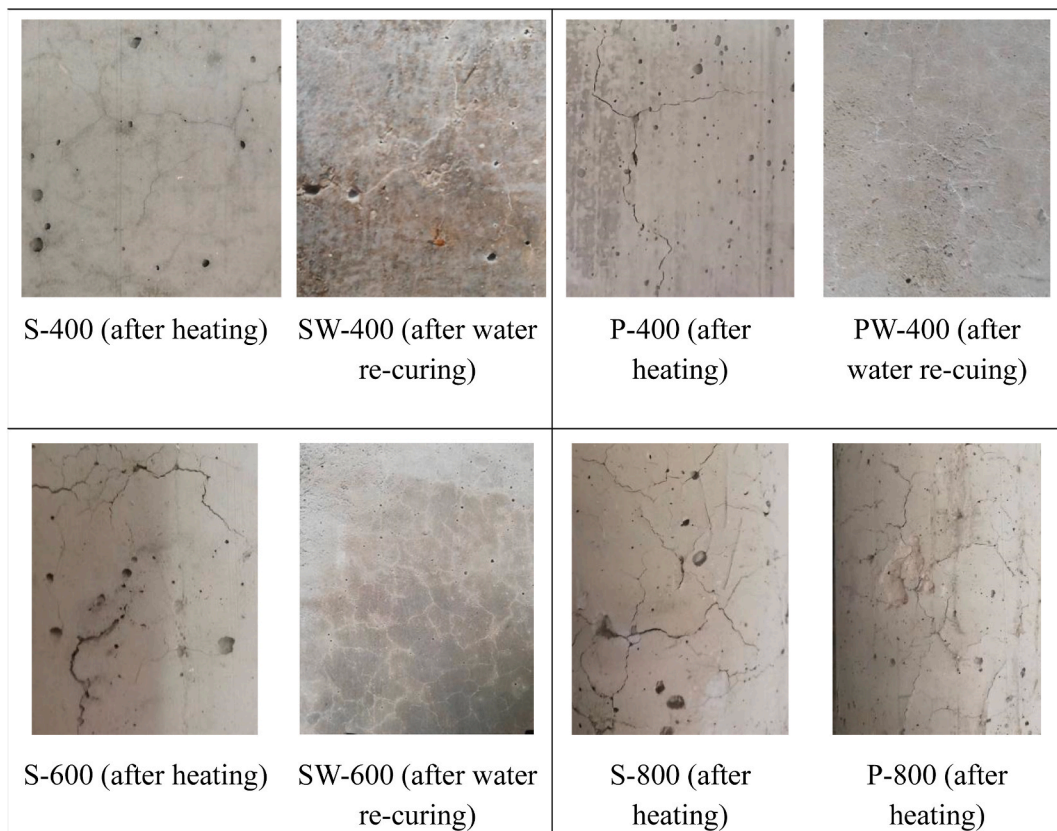
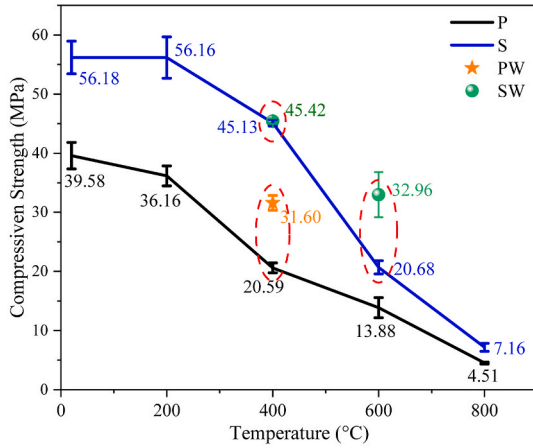
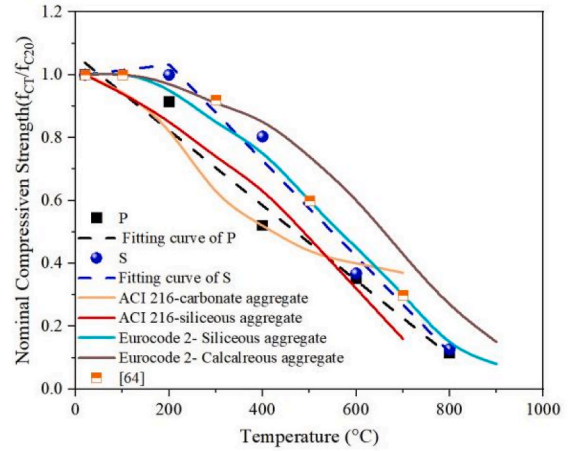


Fig. 5. Cracks morphology on the surface of the specimens after heating and water re-curing.



(a)



(b)

Fig. 6. (a) Compressive strength and (b) nominal compressive strength for different temperatures. Error bars show the standard deviation of 3 replicas.

Mix S:

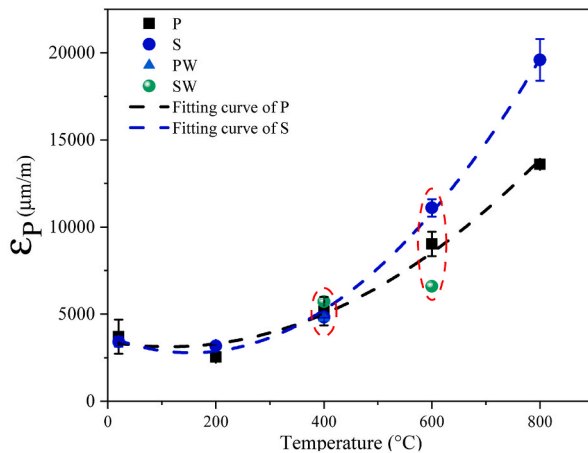
$$\frac{f_{CT}}{f_{CT0}} = \begin{cases} 1 & 20 \leq T \leq 200 & R^2 = 0.99 \\ 1.338 - 1.53 \left(\frac{T}{1000} \right) & 200 \leq T \leq 800 & R^2 = 0.98 \end{cases} \quad (2)$$

Mix P:

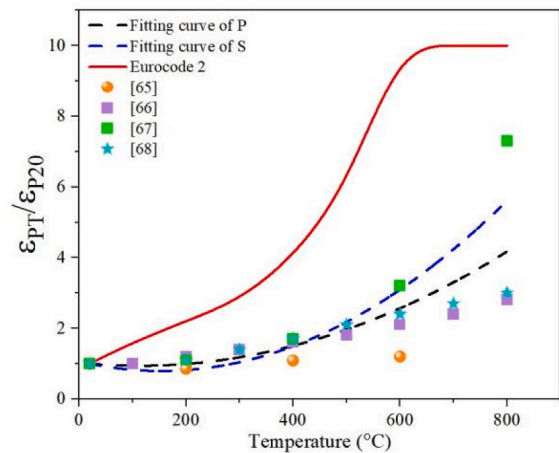
$$\frac{f_{CT}}{f_{CT0}} = 1.062 - 1.19 \left(\frac{T}{1000} \right) \quad 20 \leq T \leq 800 \quad R^2 = 0.97 \quad (3)$$

The nominal compressive strength estimated according to Eurocode 2 [32], ACI 216 [33], for siliceous aggregates, was in agreement to the proposed Eqn. (2) and Eqn. (3) (Fig. 6(b)). Moreover, the proposed Eqn. (2) fitted well the results of [64], indicating the applicability for predicting the compressive strength of thermally damaged hybrid fiber reinforced concretes.

The peak strain (ϵ_p), defined as the axial strain at the peak stress, is an essential parameter of the material. Fig. 7(a) shows the increase of peak strain with temperature, especially when it exceeded 400 °C, for both hybrid fiber reinforced concretes. Quadratic



(a)



(b)

Fig. 7. Peak strain (a) and nominal peak strain (b) at different high temperatures. Error bars show the standard deviation of 3 replicas.

functions gave the proper correlation of the peak strain and the temperature, as shown by Eqn. (4) and Eqn. (5) for Mix S and Mix P, respectively.

Mix P:

$$\varepsilon_{PT} = \varepsilon_{P20} \left(0.923 - 1.381 \left(\frac{T}{1000} \right) + 6.027 \left(\frac{T}{10} \right)^2 \right) \quad 20 \leq T \leq 800, R^2 = 0.97 \quad (4)$$

Mix S:

$$\varepsilon_{PT} = \varepsilon_{P20} \left(1.093 - 3.631 \left(\frac{T}{1000} \right) + 11.830 \left(\frac{T}{1000} \right)^2 \right) \quad 20 \leq T \leq 800, R^2 = 0.99 \quad (5)$$

Water re-curing produced a negligible effect on the peak strain for both kinds of thermally damaged hybrid fiber reinforced concrete at 400 °C, as the peak strains before and after water re-curing were similar. But water re-curing produced 40% reduction of the peak strain at 600 °C. It was attributed to the bridging effect of the re-hydrated compositions.

Fig. 7(b) compares the nominal peak strain (defined as the ratio between the peak strain of thermally damaged concrete ε_{PT} and peak strain at 20 °C ε_{P20}) by: the proposed Eqn. (4) and Eqn. (5), by the Eurocode 2 and other studies for steel fiber reinforced concretes [65–68]. Eurocode 2 overestimated the peak strain of the thermally damaged hybrid reinforced concrete. Compared to the results of other studies, the proposed equations had a good prediction over the wide temperature range up to 600 °C.

5.2. Initial elastic modulus

Fig. 8 shows the initial elastic modulus (E_{inT}) of hybrid fiber reinforced concrete under different testing scenarios. The initial elastic modulus is defined as the tangent modulus at $0.1f_{CT}$. For both hybrid fiber reinforced concretes, the initial elastic modulus decreased sharply when the temperature exceeded 200 °C. The average initial elastic modulus of Mix S and Mix P decreased from 27.54 GPa and 23.52 GPa at 20 °C to 8.86 GPa and 4.99 GPa at 400 °C, reduction of 68% and 79%, respectively. When the temperature reached 800 °C, the lowest initial elastic modulus of about 0.5 GPa was measured.

When the temperature exceeded 200 °C, the vapor pressure and thermal stress accelerated the formation and propagation of the micro cracks. Meanwhile, the decomposition of matrix produced cracks in concrete. These lead to the deterioration of the initial elastic modulus. The higher strength and bonding strength of the steel fiber can motivate the higher initial elastic modulus of Mix S than that of Mix P. But, the evolution with temperature is the similar for both thermally damaged hybrid fiber reinforced concretes. A two branches relationship (linear and exponential) between E_{inT} and the temperature was detected in the range from 20 °C to 800 °C. The proposed functions are given by Eqn. (6) and Eqn. (7).

Mix S:

$$E_{inT} = \begin{cases} E_{in20} & 20 \leq T \leq 200 \quad R^2 = 0.99 \\ E_{in20} \left(3.443 \exp \left(\frac{-6.1T}{1000} \right) \right) \pm 0.2 & 200 \leq T \leq 800 \quad R^2 = 0.99 \end{cases} \quad (6)$$

Mix P:

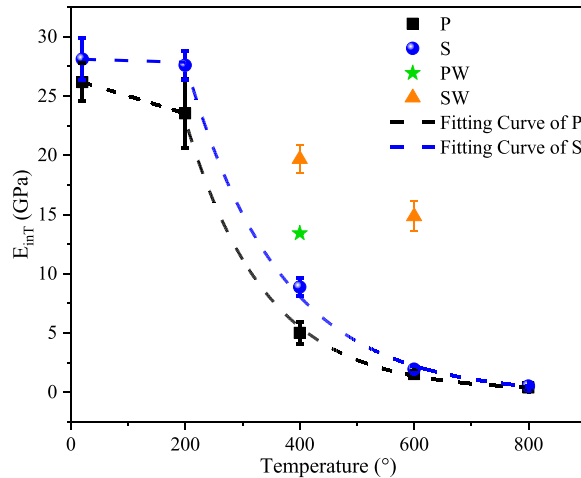


Fig. 8. Initial elastic modulus for different testing conditions. Error bars show the standard deviation of 3 replicas.

$$E_{inT} = \begin{cases} E_{in20} \left(1.011 - 0.561 \left(\frac{T}{1000} \right) \right) + 0.23 & 20 \leq T \leq 200 \\ E_{in20} \left(3.699 \exp \left(\frac{-7.2T}{1000} \right) \right) \pm 0.25 & 200 \leq T \leq 800 \end{cases} \quad R^2 = 0.99 \quad (7)$$

where T is the temperature ($^{\circ}\text{C}$), E_{in20} is the initial elastic modulus at 20°C .

Water re-curing produced a recovery effect on initial elastic modulus for both thermally damaged hybrid fiber reinforced concretes. At 400°C , the water re-curing increased the initial elastic modulus of Mix S and Mix P from 4.99 GPa and 8.86 GPa to 13.41 GPa and

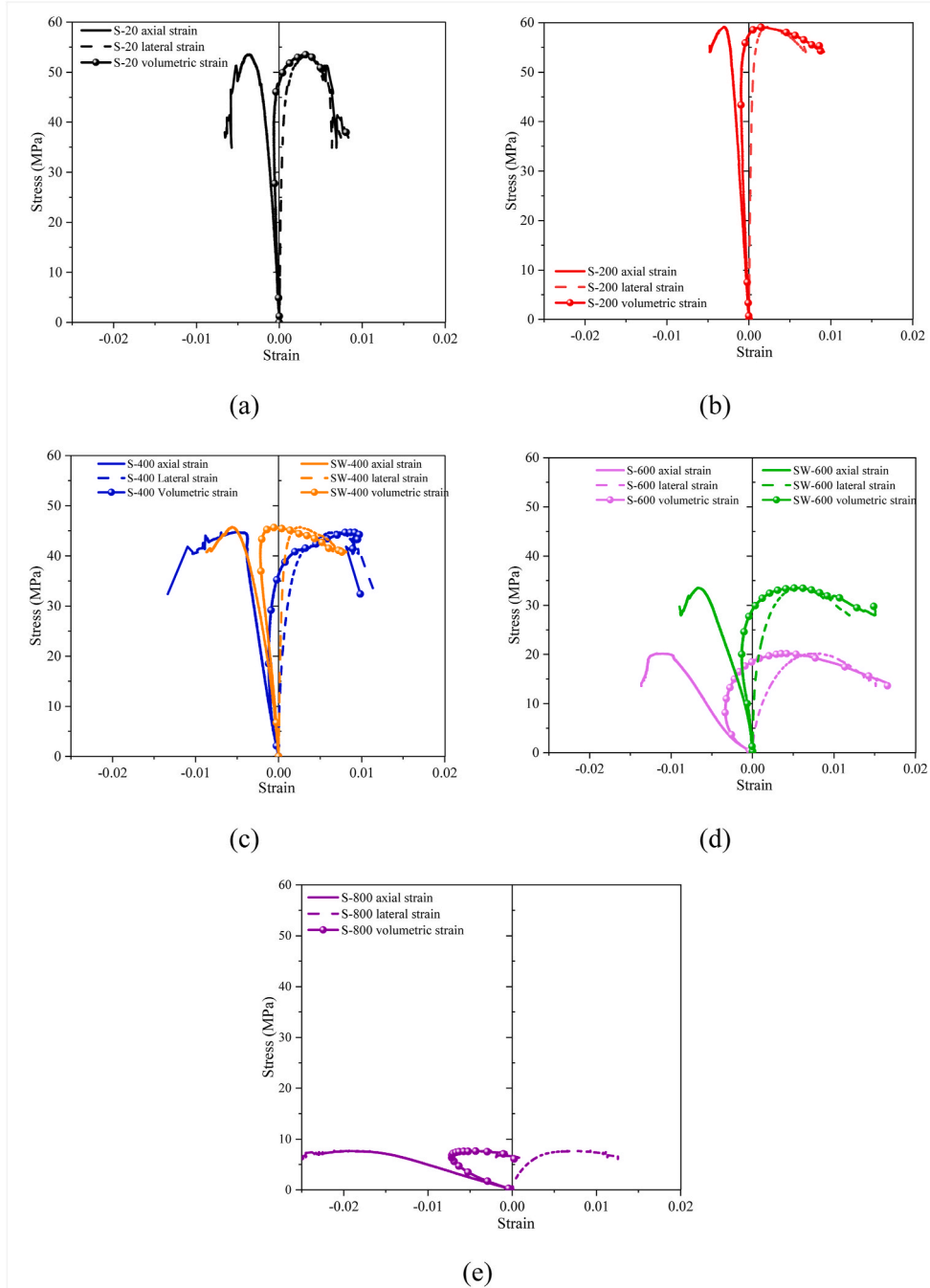


Fig. 9. Representative stress vs axial, lateral and volumetric strain curves of Mix S: (a) 20°C , (b) 200°C , (c) 400°C , (d) 600°C , and (e) 800°C .

19.67 GPa, (increase of 169% and 122%), reaching 51% and 70% of E_{in20} , respectively. During the post-heating re-curing stage, the decomposition products reacted with water and carbon dioxide, reproducing some hydrated compositions. CaO reacts with water and carbon dioxide re-generating $Ca(OH)_2$ and $CaCO_3$ [36,53]. The C_nS (such as C_2S , C_3S) reacts with water, forming C–S–H in the damaged cement matrix. The rehydrated compositions bridged or narrowed the cracks caused by the high temperature. The bonding strength of steel fiber was partially recovered [36,69]. Therefore, the extension of the micro cracks was restricted, partially recovering the initial elastic modulus of the thermally damaged hybrid fiber reinforced concrete.

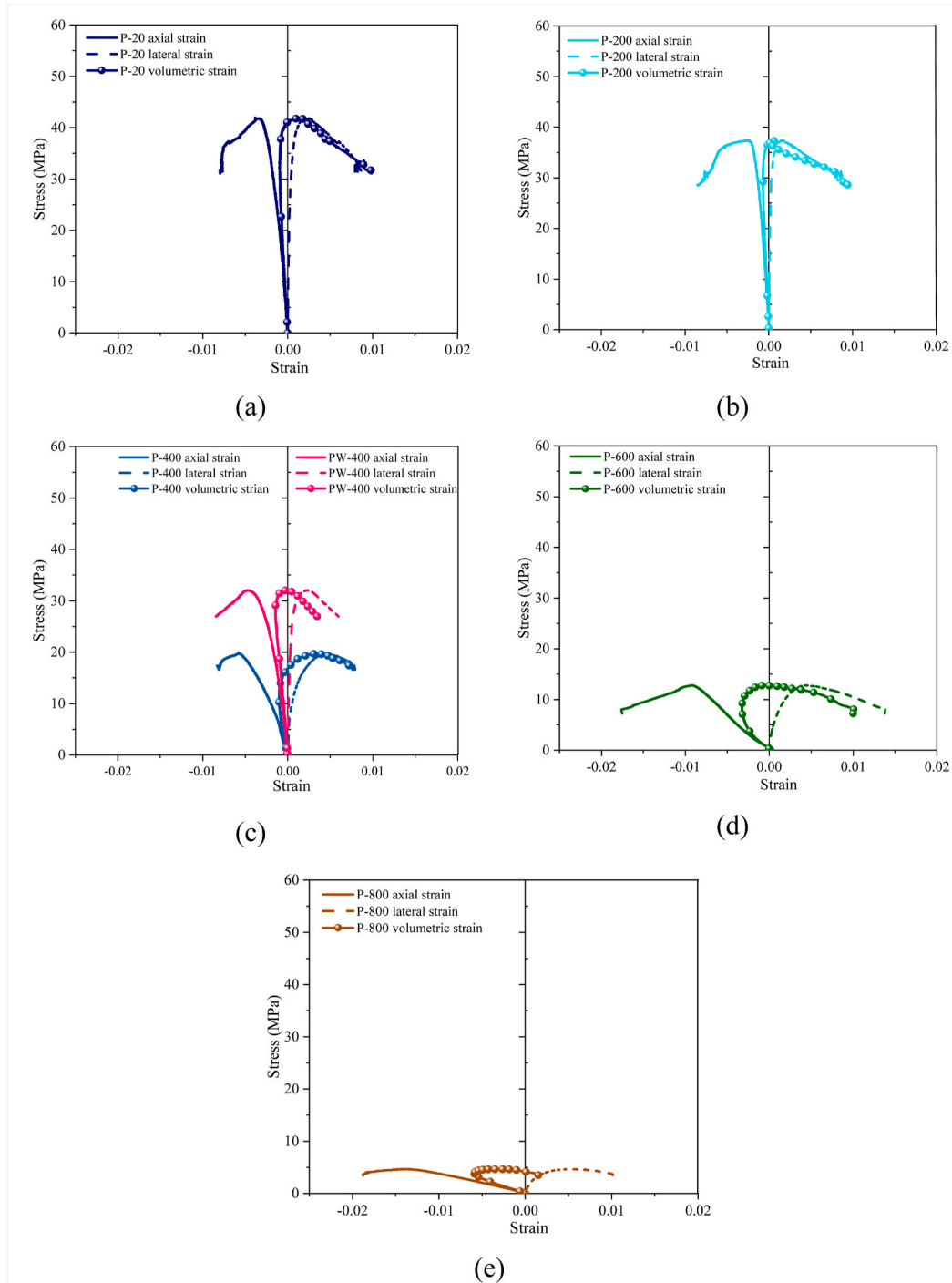


Fig. 10. Stress vs axial, lateral and volumetric strain curves for different pre-conditionings of Mix P: (a) 20 °C, (b) 200 °C, (c) 400 °C, (d) 600 °C, and (e) 800 °C.

5.3. Stress - strain relationships

The compression fracture mechanism and the stress-strain relationship are two important properties of concrete [2]. Researches [1, 9,16,22,56] on thermally damaged concrete proved that high temperature degraded the micro structure of concrete, and then changed the mechanical behavior. The micro structure affected the damage evolution, which was directly reflected by the stress-strain curve. The randomly distributed fibers in concrete produce a bridging effect on cracks, changing relationships between stress and axial strain, lateral strain, and volumetric strain. In the concrete failure theory proposed in Ref. [70], the critical load was determined according to the volume change, which represented the beginning of the internal splitting in concrete. Later, the expansion of the volume was verified to be related to the development of a continuous pattern of cracks.

Therefore, the influence of the high temperatures and water re-curing on the failure process of hybrid fiber reinforced concrete are here determined by analyzing the stress-strain curves including axial strain, lateral strain and volumetric strain.

Fig. 9 shows the stress-strain curves of Mix S under different testing scenarios. The temperatures under 200 °C had a negligible effect on stress-strain curves, except for a slight increase on compressive strength (Fig. 9(a) and (b)). The stress-strain curves showed almost linear increase and then a slight nonlinear hardening up to the peak stress. When the temperature increases to 400 °C, the stress-axial curve showed almost a linear increase to the peak stress (Fig. 9(c)). But, for stress-lateral/volumetric strain, an obvious nonlinearity appeared before peak stress. It indicated the micro structure deterioration at 400 °C. The stress-strain curves presented a large deformation when the high temperature reached 600 °C and 800 °C, showing a sharp decrease on compressive strength (Fig. 6(d) and (e)) and initial elastic modulus (Fig. 8), the increase of peak strain (Fig. 7), and a more nonlinear stress - lateral strain and stress-volumetric strain.

Water re-curing partially changed the trend of the stress-strain curves of thermally damaged concrete. At the 400 °C (Fig. 9(c)), although the water re-curing produced a negligible effect on the recovery of the stress - axial strain curve, while the stress - lateral strain and stress - volumetric strain curves showed a smaller nonlinear increase before peak load. A much stronger recovery effect was produced at 600 °C (Fig. 9(d)). The recovery effect was attributed to the rehydrated compositions. They filled and narrowed the cracks and voids, leading to the increase of the load-bearing capacity of the micro structures. The bonding strength between steel fibers and cement matrix was improved during the water re-curing.

Fig. 10 shows the stress-strain curves of Mix P at different preconditioning conditions. The high temperatures and water re-curing produced effects similar to Mix S on the stress-strain curves of Mix P. It is worth noting that water re-curing produced a stronger recovery effect on the thermally damaged Mix P. The melting and evaporation of the polypropylene fibers not only led to the loss of the bridging effect on the propagation of micro cracks, but also created micro voids for the generation and propagation of both micro and macro cracks. Rehydrated compositions produced during the water re-curing partially restored the damage and filled the voids caused by the evaporation of polypropylene fibers.

The effect of the hybrid fiber system on the stress-strain curves of thermally damaged hybrid fiber reinforced concrete is compared in Fig. 11. Mix P presented a much lower compressive strength and more softening stress-strain behavior than Mix S at 400 °C (see Fig. 11(a)). But, a less remarkable hybridization effect on the stress-strain curve at 600 °C was notable as shown in Fig. 11(b), except for the higher compressive strength. It indicated the hybrid high strength short wave-shaped fiber provided better performance of the concrete, than the polypropylene fibers. But with the increase of the temperature, the advantages gradually diminish.

Fig. 12 presents the typical stress - lateral/axial strains ratio of hybrid fiber reinforced concrete under different conditions. With the increase of the thermal damage in concrete, the lateral strain had a higher contribution to the volume strain. Water re-curing produced an obvious effect on the lateral strain. The curves of SW-400 and PW-400 shifted toward S-20 and P-20. According to the studies [2,29,

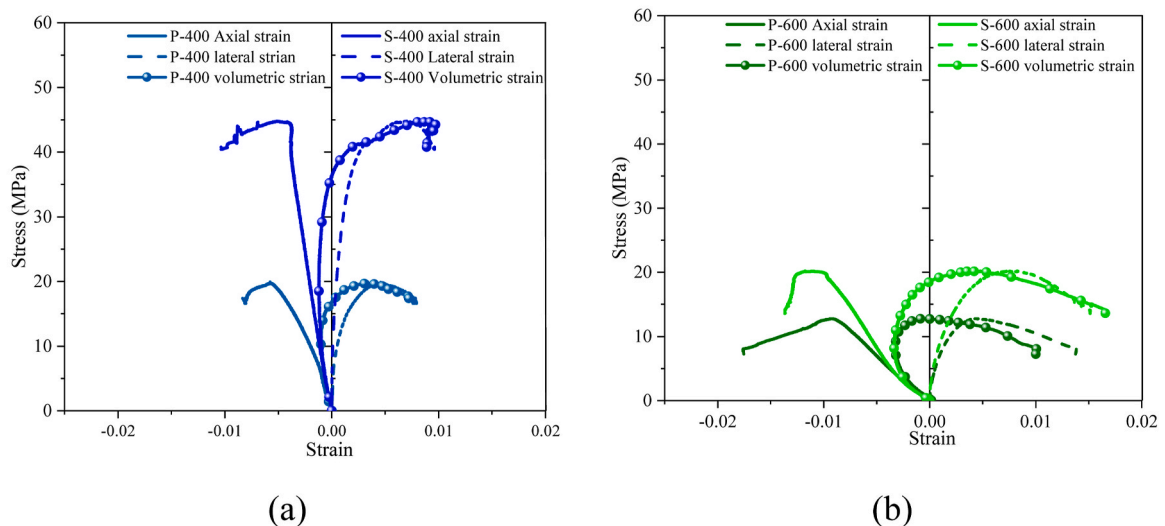


Fig. 11. Comparison of the stress-strain curves of Mix S and Mix P: (a) 400 °C and (b) 600 °C.

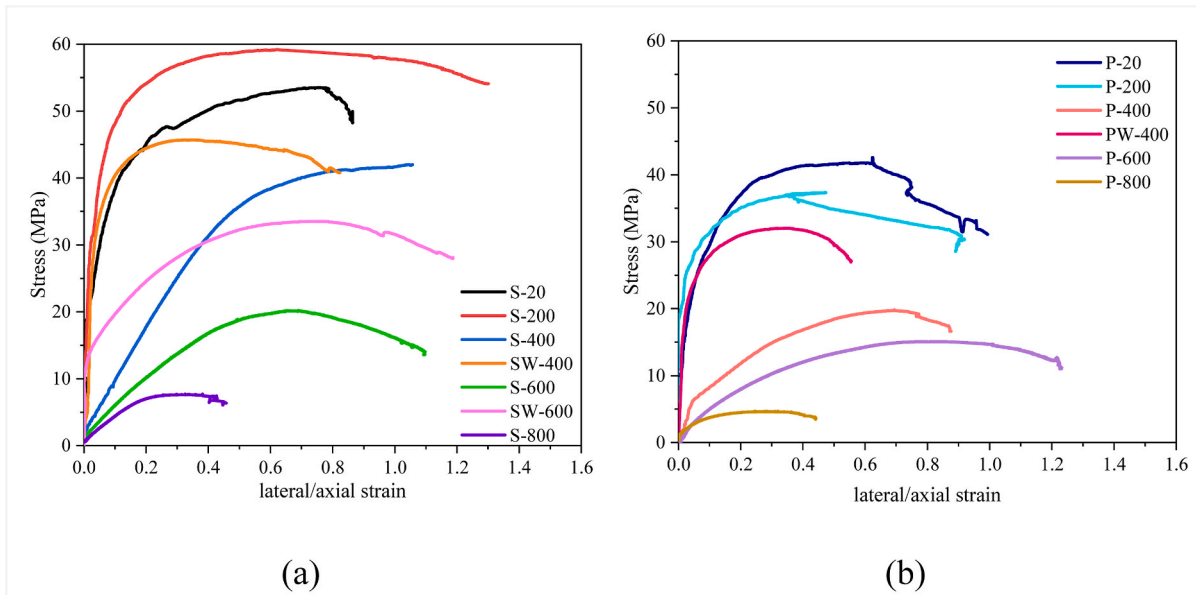


Fig. 12. Variation of the lateral/axial strains ratio with the applied stress: (a) Mix S and (b) Mix P.

30], the matrix cracks was activated at the stress point when the lateral/axial strain ratio had a clear change, which was defined as the initiation stress of the matrix crack (f_{inT}). In this study, the initiation stress is the stress at which the curve first deviates significantly from the initial linear trend.

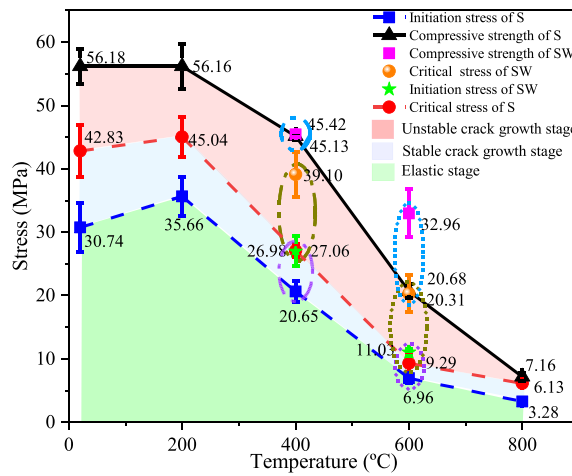
The effect of the elevated temperature and water re-curing can be quantitatively evaluated by analyzing the initiation stress (f_{inT}) and critical stress (f_{crT}). According to studies [2,29], critical stress related to the volume change of the specimen, and it was associated to the unstable cracks' extension. In this study, as in Refs. [2,29], the critical stress corresponded to the minimum volumetric strain on the stress - volumetric strain curve. Fig. 13 compares the initiation stress and critical stress of Mix S (Fig. 13(a)) and Mix P (Fig. 13(b)) under different testing conditions.

The critical stress and initiation stress of Mix S decreased with temperatures above 200 °C, with the more significant decrease in critical strength as shown in Fig. 13(a). It indicated the unstable crack propagation at a lower loading level with the increase of the thermal damage. The critical stress and initiation stress had a slight increase for temperature from 20 °C to 200 °C. It was because the vapor pressure activated the rehydration of the unhydrated cement and reduced the original defects in concrete. The initiation stress and the critical stress decreased from 35.66 MPa and 45.04 MPa at 400 °C to 6.96 MPa and 9.29 MPa at 600 °C.

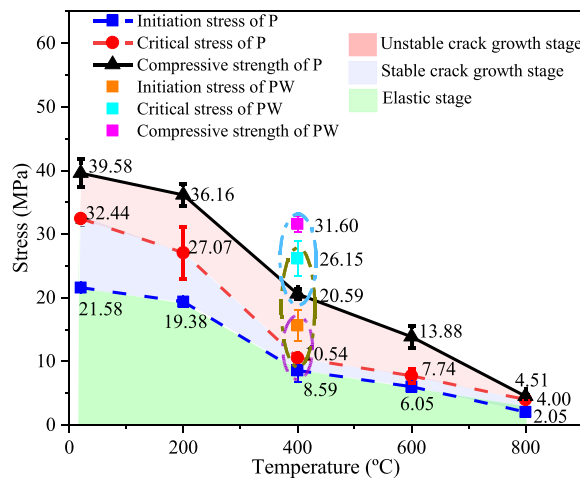
The unstable cracks growth stage was defined as the range between critical stress (f_{crT}) and compressive strength (f_{cT}), shown by the pink area in Fig. 13. The difference between f_{crT} and f_{cT} kept stable with the decrease of the compressive strength when the temperature increased from 200 °C to 600 °C, indicating the extension of unstable cracks growth stage before the pre-peak period. But the stable crack growth, defined as the area between the initiation stress (f_{inT}) and the critical stress (f_{crT}), had a significant shrinkage. It indicated the stable crack propagation was activated at a lower loading level, and propagation and coalescence of matrix cracks were faster. With the increase of the temperature, the deterioration of the micro structure of concrete led to the decrease of the loading capacity. Under external load, the micro cracks propagated and coalesced, forming the macro cracks and entering unstable crack growth stage at a low loading level.

Water re-curing partially regained the initiation stress and critical stress and extended the stable crack growth stage (see Fig. 13(a)). The initiation stress and critical stress at 400 °C (S-400) increased from 20.65 MPa and 26.98 MPa to 27.06 MPa and 39.10 MPa after water re-curing (SW-400). A more pronounced increase was produced at 600 °C. This was attributed to the rehydrated compositions, especially the C-S-H as shown in Ref. [71].

As for the internal structure performance, before the initiation stress, the micro cracks propagated mainly in ITZ (the weaker part in concrete), and concrete stayed in the elastic stage [2,72]. With the increase of load, micro cracks propagated and connect in the ITZ, then stress could not be transferred through ITZ. Some stress paths propagated into the matrix, activating the stable crack growth stage [65,70]. The hybrid fibers constrained the propagation of crack and transferred stress between cracks, extending the stable crack growth stage. The stable extension of the cracks in the matrix slightly increased the curvature of the stress-strain curve. With the increase of load, debonding of fibers and matrix occurred and cracks extended fast. The internal micro structures broke down, leading to the sharp increase of the curvature of the stress-strain curve. The specimen entered the unstable cracks growth stage. Under the high temperature environment, especially for the temperatures above 200 °C, the vapor pressure, thermal stress and decomposition increased original cracks both in ITZ and matrix before loading. The integrity and strength of ITZ were deteriorated, leading to the decrease of the initiation stress. The decomposition of hydrated components deteriorated the micro structure and weakens the bonding strength between fibers and matrix, leading to the sharp shrink of the stable crack growth stage.



(a)



(b)

Fig. 13. Initiation stress (f_{INT}), critical stress (f_{CRIT}), and compressive strength (f_{CT}) of (a) Mix S and (b) Mix P.

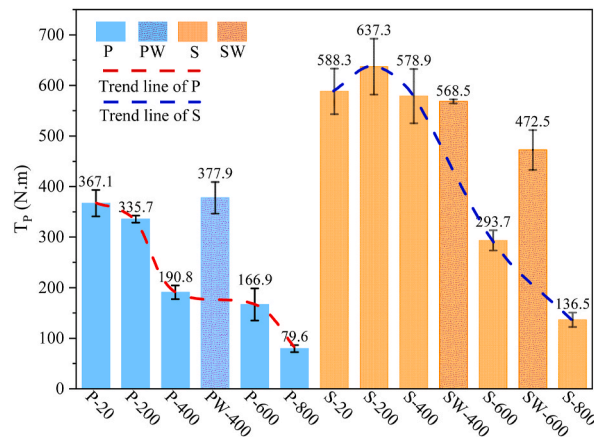


Fig. 14. Toughness of both hybrid fiber reinforced concretes at different testing conditions.

Water re-curing produced a recovery effect on the thermally damaged micro structures. During the water re-curing period, the decomposed components, produced under the high-temperature environment, re-hydrated and generated composites, like C–S–H and CaCO_3 . They filled voids, bridged or narrowed the cracks, and partially repaired the thermally damaged micro structure, leading to the increase of the integrity and strength of the micro structure. The crack bridging effect produced by hybrid fibers was enhanced by the recovery of the bonding strength.

5.4. Toughness

Toughness is a parameter to estimate the energy-absorbing ability of concrete under loading, which can be obtained by integrating the area underneath the load-displacement curve (see Eqn. (8)).

$$T = \int_0^x P(x)dx \quad (8)$$

where x is the displacement of the load cell (mm), $P(x)$ is the applied load (kN).

The toughness at the peak load (T_p) was here considered. The results of different testing conditions are summarized in Fig. 14. Elevated temperature decreased the fracture toughness of both hybrid fiber reinforced concretes. For Mix S, the fracture toughness was about 600 N m when the temperature was under 400 °C, indicating the hybrid fiber's bridging effect was not seriously deteriorated. The fracture toughness decreased by 49.3% and 76.4%, reaching 293.7 N m and 136.5 N m when temperature increased to 600 °C and 800 °C. For Mix P, the developing trend of the fracture toughness was slightly different from that of Mix S. The 200 °C produced a

Table 4
Some uniaxial compression stress-strain models for concrete.

Sargin et al. [28]	$\frac{\sigma}{f_c} = \frac{\left[A \frac{\varepsilon}{\varepsilon_p} + (B-1) \left(\frac{\varepsilon}{\varepsilon_p} \right)^2 \right]}{\left[1 + (A-2) \frac{\varepsilon}{\varepsilon_p} + B \left(\frac{\varepsilon}{\varepsilon_p} \right)^2 \right]}$	$A = \frac{E_{in}}{E_p}$ $B = 0.65 - 7.25f_c \times 10^{-3}$
Wang et al. [73]	$\frac{\sigma}{f_c} = \frac{\left[A \frac{\varepsilon}{\varepsilon_p} + B \left(\frac{\varepsilon}{\varepsilon_p} \right)^2 \right]}{\left[1 + C \frac{\varepsilon}{\varepsilon_p} + D \left(\frac{\varepsilon}{\varepsilon_p} \right)^2 \right]}$	A, B, C and D are factors that controls the ascending and descending branches
Van Gysel et al. [27]	$\frac{\sigma}{f_c} = \begin{cases} \frac{\left[N \frac{\varepsilon}{\varepsilon_p} - N \left(\frac{\varepsilon}{\varepsilon_p} \right)^2 \right]}{\left[1 + (N-2) \frac{\varepsilon}{\varepsilon_p} \right]} \\ \frac{1}{\left[1 + \left(\frac{\varepsilon - \varepsilon_p}{(K-1)\varepsilon_p} \right)^2 \right]} \end{cases}$ $0 \leq \frac{\varepsilon}{\varepsilon_p} \leq K$ $K \leq \frac{\varepsilon}{\varepsilon_p}$	$N = \frac{E_{in}}{E_p}$ $K = 0.5[(0.5N+1) + ((0.5N+1)^2 - 2)^{0.5}]$
Popovics et al. [74]	$\frac{\sigma}{f_c} = \frac{\beta \frac{\varepsilon}{\varepsilon_p}}{\beta - 1 + \left(\frac{\varepsilon}{\varepsilon_p} \right)^\beta}$	$\beta = \frac{1}{1 - \frac{f_c}{\varepsilon_p E_{in}}}$
Tomaszewicz et al. [75]	$\frac{\sigma}{f_c} = \begin{cases} \frac{\beta \frac{\varepsilon}{\varepsilon_p}}{\beta - 1 + \left(\frac{\varepsilon}{\varepsilon_p} \right)^\beta}, & 0 \leq \frac{\varepsilon}{\varepsilon_p} \leq 1 \\ \frac{\beta \frac{\varepsilon}{\varepsilon_p}}{\beta - 1 + \left(\frac{\varepsilon}{\varepsilon_p} \right)^{k\beta}}, & \frac{\varepsilon}{\varepsilon_p} \geq 1 \end{cases}$	$\beta = \frac{8.32}{8.32 - (f_c)^{0.475}} k = \frac{f_c}{20}$
Tsai et al. [76]	$\frac{\sigma}{f_c} = \frac{m \frac{\varepsilon}{\varepsilon_p}}{1 + \left(m - \frac{n}{n-1} \right) \frac{\varepsilon}{\varepsilon_p} + \left(\frac{1}{n-1} \right) \left(\frac{\varepsilon}{\varepsilon_p} \right)^n}$	$m = 1 + \frac{17.9}{f_c}$ $n = \frac{f_c}{6.668} - 1.85$
Wee et al. [77]	$\frac{\sigma}{f_c} = \frac{n\beta \frac{\varepsilon}{\varepsilon_p}}{n\beta - 1 + \left(\frac{\varepsilon}{\varepsilon_p} \right)^{m\beta}}$	$m = 1, n = 1 \quad f_c \leq 50$ $\beta = \frac{1}{1 - \frac{f_c}{\varepsilon_p E_{in}}} \quad m = \left(\frac{50}{f_c} \right)^3, n = \left(\frac{50}{f_c} \right)^{1.3} \quad f_c \geq 50$
Tulin and Gerstle [78]	$\frac{\sigma}{f_c} = \frac{3 \frac{\varepsilon}{\varepsilon_p}}{2 + \left(\frac{\varepsilon}{\varepsilon_p} \right)^3}$	

slightly reduction in fracture toughness. When the temperature increased to 400 °C, the fracture toughness decreased by 48.0%, reaching 190.8 N m. The melting and evaporation of the polypropylene fibers reduced the bridging effect on the propagation of cracks, especially for the micro cracks, reducing the load-bearing capacity.

Water re-curing improved the energy absorbing ability of both thermally damaged hybrid fiber reinforced concretes. At 400 °C, after water re-curing, the fracture toughness recovered to the un-thermally damaged level. And, at 600 °C, the fracture toughness increased from 293.7 N m (S-600) to 472.5 N m (SW-600), reaching 80% of S-20.

6. Prediction of the stress-axial strain relation

6.1. Selection of available predictive models

Numerous predictive models for the stress - strain relationship of concrete under uniaxial compression were developed. Some of them are listed in Table 4.

These models were used for the analysis of the thermally damaged concrete. The models presented in Refs. [27,28,73] were effective to predict the stress-strain relationship for undamaged and thermally damaged concrete. But, it is not easy to find the proper parameters. The models detailed in Refs. [74–76] are simpler. Parameters, which can be determined easily, were introduced for the post-peak curve of the thermally damaged concrete. However, hybrid fiber and elevated temperatures influence the mechanical performance, leading to some changes on the stress-axial curve of the reinforced concrete. Therefore, the proposed models were not effective for predicting the stress-strain curve of the thermally damaged hybrid fiber reinforced concrete. In this study, the model proposed by Wee et al. [77] was adopted as the basic model for predicting the stress-strain relationship of thermally damaged concrete. Some parameters were redefined, for higher accuracy, as:

$$\sigma = \frac{n_1 \beta \frac{\epsilon}{\epsilon_{PT}}}{n_1 \beta - 1 + \left(\frac{\epsilon}{\epsilon_{PT}}\right)^{n_2} \beta f_{cT}} f_{cT} \quad (9)$$

$$\beta = \frac{1}{1 - \frac{f_{cT}}{\epsilon_{PT} E_{inT}}} \quad (10)$$

where σ is the compressive stress (MPa), ϵ is axial strain, f_{cT} is the compressive strength of the thermally damaged concrete, ϵ_{PT} is the strain of the thermally damaged concrete at peak load, β is the material parameter that depends on the shape of the stress-strain diagram, E_{inT} is the initial tangent modulus, n_1 and n_2 are factors dependent on the temperature that can be determined according to the testing results as shown by Eqn. (11) and Eqn. (12):

Mix S:

$$\begin{aligned} n_1 = n_2 = 1, \quad 0 \leq \frac{\epsilon}{\epsilon_{PT}} \leq 1 \\ n_1 = 0.80 + 0.94 \sin\left(\pi \left(\frac{T + 147.38}{318.89}\right)\right) \pm 0.03 \\ n_2 = 0.67 + 0.73 \sin\left(\pi \left(\frac{T + 154.40}{341.37}\right)\right) \pm 0.03 \end{aligned} \quad \frac{\epsilon}{\epsilon_{PT}} \geq 1 \quad (11)$$

Mix P:

$$\begin{aligned} n_1 = n_2 = 1, \quad 0 \leq \frac{\epsilon}{\epsilon_{PT}} \leq 1 \\ n_1 = \begin{cases} 0.63 + 1.78 \left(\frac{T}{1000}\right) - 2.58 \left(\frac{T}{1000}\right)^2 \pm 0.02 \\ 6.08 - 19.1 \left(\frac{T}{1000}\right) + 15.46 \left(\frac{T}{1000}\right)^2 \pm 0.02 \end{cases} \quad 20 \leq T \leq 400 \\ n_2 = \begin{cases} 0.67 + 0.92 \left(\frac{T}{1000}\right) \pm 0.03 \\ 1.98 - 2.56 \left(\frac{T}{1000}\right) \pm 0.03 \end{cases} \quad \begin{matrix} 20 \leq T \leq 400 \\ 400 \leq T \leq 800 \end{matrix} \end{aligned} \quad \frac{\epsilon}{\epsilon_{PT}} \geq 1 \quad (12)$$

6.2. Assessment of the adopted model

For a given hybrid fiber reinforced concrete, f_{c20} , ϵ_{PT} and E_{in20} can be determined by room temperature laboratory testing. According to Eqns. (2)–(7) and Eqns. (9)–(12), f_{cT} , ϵ_{PT} , E_{inT} , n_1 , and n_2 can be obtained. Then, the stress-strain curve of the thermally damaged hybrid fiber reinforced concrete can be determined. Fig. 15 shows the comparison between predicted stress-strain curves and experimental results. The model provided a good prediction to the experimental stress-strain curves of thermally damaged concrete. The differences in some testing conditions, such as S-400 and P-200 were caused by the accuracy on f_{cT} and ϵ_{PT} , but the stress

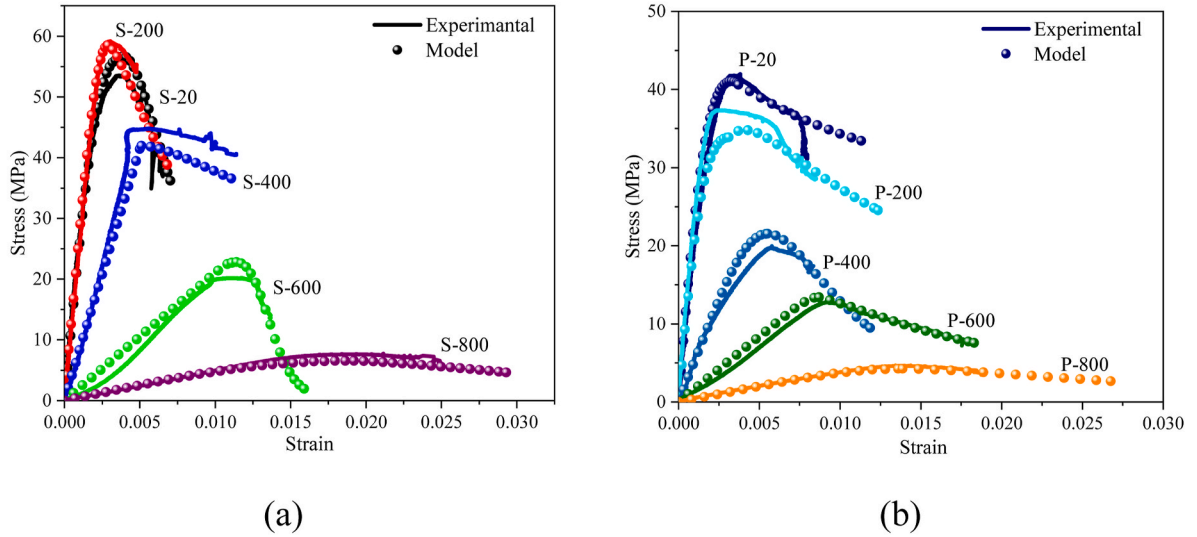


Fig. 15. Comparison of predicted stress - strain curves and experimental results of (a) Mix S and (b) Mix P.

underestimations are lower than 10%.

To evaluate the effectiveness of the model for water re-curing thermally damaged concrete, the comparison between predicted stress - strain curves and experimental ones is shown in Fig. 16. According to the testing data, the relationships in Table 5 were used for the prediction.

As shown in Fig. 16, the model had a good prediction for PW-400, while it is not for SW-400 and SW-600. The latter could mainly depend on the low accuracy of the parameters determined (see Table 5), due to the limited data. Therefore, more experimental measurements are needed to improve the accuracy of the model adopted for the water re-cured thermally damaged hybrid fiber reinforced concrete.

7. Conclusions

In this study, the effect of the elevated temperature and water re-curing on the compression mechanical performance of two hybrid fiber reinforced concretes were investigated. Based on the results and analysis, the following conclusions can be drawn.

- (1) The temperatures above 200 °C decreased the compressive strength, initial elastic modulus, peak strain, and fracture toughness of both hybrid fiber reinforced concretes. But, hybrid fiber reinforced concrete including high strength short steel fibers (S) had higher compressive strength, initial elastic modulus, and fracture toughness than mix with polypropylene fiber any high temperature exposition.

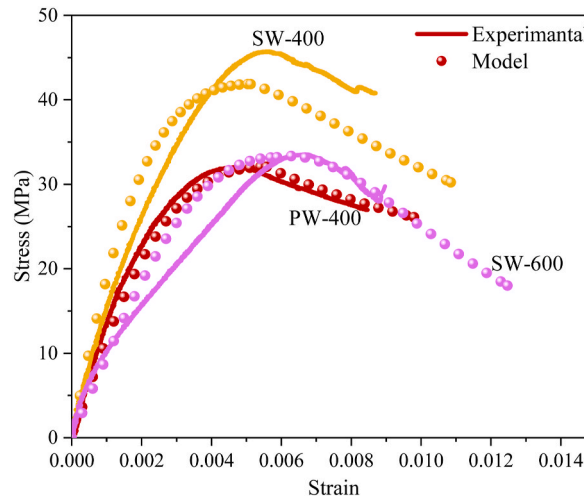


Fig. 16. Comparison of predicted stress-strain curves and experimental results of water re-curing thermally damaged concrete.

Table 5
Parameters for the prediction of stress-strain curve of SW-400, SW-600, and PW-400.

SW-400	SW-600	PW-400
$f_{cW400} = f_{c400}$	$f_{cW600} = 1.4f_{c600}$	$f_{cW400} = 1.5f_{c400}$
$\varepsilon_{PW400} = 0.9\varepsilon_{P400}$	$\varepsilon_{PW600} = 0.56\varepsilon_{P400}$	$\varepsilon_{PW400} = \varepsilon_{P400}$
$E_{inW400} = 2.4E_{inW400}$	$E_{inW600} = 5.0E_{in600}$	$E_{inW400} = 2.5E_{inW400}$
$n_{1-W400} = 0.6n_{1-20}$	$n_{1-W600} = n_{1-20}$	$n_{1-W400} = n_{1-20}$
$n_{2-W400} = 0.75n_{2-20}$	$n_{2-W600} = n_{2-20}$	$n_{2-W400} = 1.1n_{2-20}$

f_c is the compressive strength; ε_p is the peak strain; E_{in} is the initial elastic modulus; n_1 and n_2 are the two factors in Eqn. (9).

- (2) Damage initiation stress and critical stress decreased with the increase of temperature above 200 °C. The stable crack growth stage was shrunk when the temperature increased from 200 to 600 °C, while the unstable crack growth stage was extended. Hybrid fiber reinforced concrete including short steel fibers (S) has higher initiation stress and critical stress than mix with polypropylene fiber. Water re-curing partially regained the initiation stress and critical stress and extended the stable crack growth stage.
- (3) The adapted available model was effective for predicting the stress-strain curve of both thermally damaged hybrid fiber reinforced concretes. But improvement is needed for predicting the stress-axial strain curve of the water re-cured thermally damaged hybrid fiber reinforced concrete. It needs a wider dataset for setting the required parameters.
- (4) Overall, this study provided insight into the thermal damage evolution and compressive stress-strain relationship of hybrid fiber reinforced concretes with different levels of temperature exposition. Moreover, the advantages of the water re-curing were proved in recovering the thermal damage and improving the compressive performance of the considered hybrid fiber reinforced concretes. The findings in this study would be helpful for repairing such thermally damage hybrid fiber reinforced concretes and also for assessing the accuracy of dedicated numerical predictions.

CRediT authorship contribution statement

Fengzhen He: Conceptualization, Investigation, Methodology, Data curation, Formal analysis, Validation, Writing – original draft, Writing – review & editing. **Luigi Biolzi:** Conceptualization, Investigation, Methodology, Validation, Supervision, Writing – review & editing, Project administration. **Valter Carvelli:** Investigation, Methodology, Formal analysis, Validation, Writing – review & editing.

Declaration of competing interest

The authors declare that they have no known competing financial interests or personal relationships that could have appeared to influence the work reported in this paper.

Data availability

Data will be made available on request.

Acknowledgements

The authors gratefully acknowledge TEKNA CHEM S.p.A. (Renate, IT) and Mr. Silvio Cocco and Dr Valeria Campioni for the support to the research. Special thanks are due to Mr. Daniele Spinelli (Materials Testing Laboratory, Politecnico di Milano) who supervised F. He in setting up the experimental apparatus and performing the tests. F. He acknowledges the China Scholarship Council Grant and Key University Science Research Project of Jiangsu Province (20KJA560002).

References

- [1] B. Chen, J. Liu, Residual strength of hybrid-fiber-reinforced high-strength concrete after exposure to high temperatures, *Cement Concr. Res.* 34 (6) (2004) 1065–1069.
- [2] G.M. Giaccio, R.L. Zerbin, Mechanical behaviour of thermally damaged high-strength steel fibre reinforced concrete, *Mater. Struct.* 38 (3) (2005) 335–342.
- [3] G. Sanjayan, L.J. Stocks, Spalling of high-strength silica fume concrete in fire, *Materials Journal* 90 (2) (1993) 170–173.
- [4] F. Ulm, O. Coussy, Z.P. Bazant, The “Chunnel” fire. I: chemoplastic softening in rapidly heated concrete, *J. Eng. Mech.* 125 (3) (1999) 272–282.
- [5] Z.P. Baïant, B. Io, Analysis of Pore Pressure, Thermal Stress and Fracture in Rapidly Heated Concrete, 1997.
- [6] M. Ozawa, S. Uchida, T. Kamada, H. Morimoto, Study of mechanisms of explosive spalling in high-strength concrete at high temperatures using acoustic emission, *Construct. Build. Mater.* 37 (2012) 621–628.
- [7] B. Demirel, O. Keleştemur, Effect of elevated temperature on the mechanical properties of concrete produced with finely ground pumice and silica fume, *Fire Saf. J.* 45 (6–8) (2010) 385–391.
- [8] Z. Xing, A. Beaucour, R. Hebert, A. Noumowe, B. Ledesert, Influence of the nature of aggregates on the behaviour of concrete subjected to elevated temperature, *Cement Concr. Res.* 41 (4) (2011) 392–402.
- [9] R. Serrano, A. Cobo, M.I. Prieto, M. de Las Nieves González, Analysis of fire resistance of concrete with polypropylene or steel fibers, *Construct. Build. Mater.* 122 (2016) 302–309.
- [10] J.F. Dong, Q.Y. Wang, Z.W. Guan, H.K. Chai, High-temperature behaviour of basalt fibre reinforced concrete made with recycled aggregates from earthquake waste, *J. Build. Eng.* 48 (2022), 103895, <https://doi.org/10.1016/j.jobe.2021.103895>.
- [11] J. Bošnjak, J. Ozbolt, R. Hahn, Permeability measurement on high strength concrete without and with polypropylene fibers at elevated temperatures using a new test setup, *Cement Concr. Res.* 53 (2013) 104–111.

- [12] Y. Ding, C. Zhang, M. Cao, Y. Zhang, C. Azevedo, Influence of different fibers on the change of pore pressure of self-consolidating concrete exposed to fire, *Construct. Build. Mater.* 113 (2016) 456–469.
- [13] P. Nuaklong, N. Boonchoo, P. Jongvivatsukul, T. Charinpanitkul, P. Sukontasukkul, Hybrid effect of carbon nanotubes and polypropylene fibers on mechanical properties and fire resistance of cement mortar, *Construct. Build. Mater.* 275 (2021), 122189.
- [14] H. Wu, X. Lin, A. Zhou, A review of mechanical properties of fibre reinforced concrete at elevated temperatures, *Cement Concr. Res.* 135 (2020), 106117.
- [15] C.S. Poon, Z.H. Shui, L. Lam, Compressive behavior of fiber reinforced high-performance concrete subjected to elevated temperatures, *Cement Concr. Res.* 34 (12) (2004) 2215–2222.
- [16] P.S. Song, S. Hwang, Mechanical properties of high-strength steel fiber-reinforced concrete, *Construct. Build. Mater.* 18 (9) (2004) 669–673.
- [17] H.T. Wang, L.C. Wang, Experimental study on static and dynamic mechanical properties of steel fiber reinforced lightweight aggregate concrete, *Construct. Build. Mater.* 38 (2013) 1146–1151.
- [18] R.S. Olivito, F.A. Zuccarello, An experimental study on the tensile strength of steel fiber reinforced concrete, *Compos. B Eng.* 41 (3) (2010) 246–255.
- [19] N. Banthia, M. Sappakittipakorn, Toughness enhancement in steel fiber reinforced concrete through fiber hybridization, *Cement Concr. Res.* 37 (9) (2007) 1366–1372.
- [20] L. Jin, R. Zhang, G. Dou, X. Du, Fire resistance of steel fiber reinforced concrete beams after low-velocity impact loading, *Fire Saf. J.* 98 (2018) 24–37.
- [21] R. Fike, V. Kodur, Enhancing the fire resistance of composite floor assemblies through the use of steel fiber reinforced concrete, *Eng. Struct.* 33 (10) (2011) 2870–2878.
- [22] Y. Li, K.H. Tan, E. Yang, Synergistic effects of hybrid polypropylene and steel fibers on explosive spalling prevention of ultra-high performance concrete at elevated temperature, *Cement Concr. Compos.* 96 (2019) 174–181.
- [23] W. Zheng, H. Li, Y. Wang, Compressive behaviour of hybrid fiber-reinforced reactive powder concrete after high temperature, *Mater. Des.* 41 (2012) 403–409.
- [24] D. Vafaei, X. Ma, R. Hassani, J. Duan, Y. Zhuge, Microstructural and mechanical properties of fiber-reinforced seawater sea-sand concrete under elevated temperatures, *J. Build. Eng.* 50 (2022), 104140, <https://doi.org/10.1016/j.jobe.2022.104140>.
- [25] G.M. Giaccio, R.L. Zerbino, Mechanical behaviour of thermally damaged high-strength steel fibre reinforced concrete, *Mater. Struct.* 38 (3) (2005) 335–342.
- [26] D.J. Carneira, K. Chu, Stress-strain relationship for plain concrete in compression, *J. Proc.* (1985) 797–804.
- [27] A. Van Gysel, L. Taerwe, Analytical formulation of the complete stress-strain curve for high strength concrete, *Mater. Struct.* 29 (9) (1996) 529–533.
- [28] M. Sargin, S.K. Ghosh, V.K. Handa, Effects of lateral reinforcement upon the strength and deformation properties of concrete, *Mag. Concr. Res.* 23 (75–76) (1971) 99–110.
- [29] B. Barragán, A. Di Maio, G. Giaccio, L. Traversa, R. Zerbino, Effects of High Temperature on Residual, Mechanical, and Transport Properties of Concrete, vol. 192, Special Publication, 2000, pp. 983–1000.
- [30] S.P. Shah, S. Chandra, Critical stress, volume change, and microcracking of concrete, *J. Proc.* (1968) 770–780.
- [31] G. Giaccio, C. Rocco, D. Violini, J. Zappitelli, R. Zerbino, High-strength concretes incorporating different coarse aggregates, *Materials Journal* 89 (3) (1992) 242–246.
- [32] EN 1992-1-2:2004+A1, Eurocode 2: Design of Concrete Structures - Part 1-2: General Rules - Structural Fire Design, 2019.
- [33] ACI 216-Code Requirements for Determining Fire Resistance of Concrete and Masonry Construction Assemblies.
- [34] C.A.O. Finland, High Strength Concrete Supplementary Rules and Fire Design, RakMK B4, Concrete Association of Finland Finland, 1991.
- [35] Y. Lin, C. Hsiao, H. Yang, Y. Lin, The effect of post-fire-curing on strength-velocity relationship for nondestructive assessment of fire-damaged concrete strength, *Fire Saf. J.* 46 (4) (2011) 178–185.
- [36] A.H. Akca, N. Özyurt, Deterioration and recovery of FRC after high temperature exposure, *Cement Concr. Compos.* 93 (2018) 260–273.
- [37] A.A. Awal, I.A. Shehu, M. Ismail, Effect of cooling regime on the residual performance of high-volume palm oil fuel ash concrete exposed to high temperatures, *Construct. Build. Mater.* 98 (2015) 875–883.
- [38] A. Mendes, J.G. Sanjayan, F. Collins, Effects of slag and cooling method on the progressive deterioration of concrete after exposure to elevated temperatures as in a fire event, *Mater. Struct.* 44 (3) (2011) 709–718.
- [39] T. Horiguchi, S.L. Suhaendi, Recovery behavior of hybrid fiber reinforced high strength concrete after fire exposure, *J. Struct. Fire Eng.* (2010).
- [40] A.S.M.A. Awal, I.A. Shehu, M. Ismail, Effect of cooling regime on the residual performance of high-volume palm oil fuel ash concrete exposed to high temperatures, *Construct. Build. Mater.* 98 (2015) 875–883, <https://doi.org/10.1016/j.conbuildmat.2015.09.001>.
- [41] Y. Lin, C. Hsiao, H. Yang, Y. Lin, The effect of post-fire-curing on strength-velocity relationship for nondestructive assessment of fire-damaged concrete strength, *Fire Saf. J.* 46 (4) (2011) 178–185, <https://doi.org/10.1016/j.firesaf.2011.01.006>.
- [42] T. Horiguchi, S.L. Suhaendi, Recovery behavior of hybrid fiber reinforced high strength concrete after fire exposure, *J. Struct. Fire Eng.* 1 (4) (2010) 219–229, <https://doi.org/10.1260/2040-2317.1.4.219>.
- [43] Aeternum Proof, TEKNA CHEM S.p.A. https://www.teknachemgroup.com/public/allegato/st_aeternum_proof_v2020rev1_en.pdf.
- [44] S. Cattaneo, F. Mola, Assessing the quality control of self-consolidating concrete properties, *J. Construct. Eng. Manag.* 138 (2) (2012) 197–205.
- [45] F. He, L. Biolzi, V. Carvelli, Effect of fiber hybridization on mechanical properties of concrete, *Mater. Struct.* 55 (7) (2022) 195, <https://doi.org/10.1617/s11527-022-02020-9>.
- [46] EN 12390-2, Testing Hardened Concrete, Part 2: Making and Curing Specimens for Strength Test, 2019.
- [47] EN 12390-3, Testing Hardened Concrete, Part 3: Compressive Strength of Test Specimens, 2019.
- [48] C. Poon, S. Azhar, M. Anson, Y. Wong, Strength and durability recovery of fire-damaged concrete after post-fire-curing, *Cement Concr. Res.* 31 (9) (2001) 1307–1318.
- [49] EN 12504-4, Testing Concrete in Structures Part 4: Determination of Ultrasonic Pulse Velocity, 2021.
- [50] Y.N. Chan, X. Luo, W. Sun, Compressive strength and pore structure of high-performance concrete after exposure to high temperature up to 800 C, *Cement Concr. Res.* 30 (2) (2000) 247–251.
- [51] J. Lee, Y. Xi, K. Willam, Properties of concrete after high-temperature heating and cooling, *ACI Mater. J.* 105 (4) (2008) 334.
- [52] Y. Zhang, H. Liu, C. Zhao, J.W. Ju, M. Bauchy, Deconstructing water sorption isotherms in cement pastes by lattice density functional theory simulations, *J. Am. Ceram. Soc.* 104 (8) (2021) 4226–4238.
- [53] Y. Zhang, Q. Zhou, J.W. Ju, M. Bauchy, New insights into the mechanism governing the elasticity of calcium silicate hydrate gels exposed to high temperature: a molecular dynamics study, *Cement Concr. Res.* 141 (2021), 106333.
- [54] C. Alonso, L. Fernandez, Dehydration and rehydration processes of cement paste exposed to high temperature environments, *J. Mater. Sci.* 39 (9) (2004) 3015–3024.
- [55] K. Komlos, S. Popovics, T. Nürnbergerová, B. Babal, J.S. Popovics, Ultrasonic pulse velocity test of concrete properties as specified in various standards, *Cement Concr. Compos.* 18 (5) (1996) 357–364.
- [56] M. Nematzadeh, M. Tayebi, H. Samadvand, Prediction of ultrasonic pulse velocity in steel fiber-reinforced concrete containing nylon granule and natural zeolite after exposure to elevated temperatures, *Construct. Build. Mater.* 273 (2021), 121958.
- [57] L.I. Knab, G.V. Blessing, J.R. Clifton, Laboratory evaluation of ultrasonics for crack detection in concrete, *J. Proc.* (1983) 17–27.
- [58] H.J. Yim, S. Park, J.H. Kim, H. Kwak, Nonlinear ultrasonic method to evaluate residual mechanical properties of thermally damaged concrete, *ACI Mater. J.* 111 (4) (2014) 399.
- [59] A.Y. Nuran, I.B. Topçu, The influence of silicoferrochromium fume on concrete properties, *Cement Concr. Res.* 25 (2) (1995) 387–394.
- [60] M. Zeiml, D. Leithner, R. Lackner, H.A. Mang, How do polypropylene fibers improve the spalling behavior of in-situ concrete? *Cement Concr. Res.* 36 (5) (2006) 929–942.
- [61] Y. Zhang, J.W. Ju, H. Zhu, Z. Yan, A novel multi-scale model for predicting the thermal damage of hybrid fiber-reinforced concrete, *Int. J. Damage Mech.* 29 (1) (2020) 19–44.

- [62] O. Dügenci, T. Haktanir, F. Altun, Experimental research for the effect of high temperature on the mechanical properties of steel fiber-reinforced concrete, *Construct. Build. Mater.* 75 (2015) 82–88.
- [63] J.B. Odelson, E.A. Kerr, W. Vichit-Vadakan, Young's modulus of cement paste at elevated temperatures, *Cement Concr. Res.* 37 (2) (2007) 258–263.
- [64] J. Kim, G. Lee, Evaluation of mechanical properties of steel-fibre-reinforced concrete exposed to high temperatures by double-punch test, *Construct. Build. Mater.* 79 (2015) 182–191.
- [65] Z. Lu, A Research on Fire Response of Reinforced Concrete Beams, Tongji University, Shanghai, 1989.
- [66] F. Aslani, B. Samali, Constitutive relationships for steel fibre reinforced concrete at elevated temperatures, *Fire Technol.* 50 (5) (2014) 1249–1268.
- [67] W. Zheng, B. Luo, Y. Wang, Stress-strain relationship of steel-fibre reinforced reactive powder concrete at elevated temperatures, *Mater. Struct.* 48 (7) (2015) 2299–2314.
- [68] Y. Tai, H. Pan, Y. Kung, Mechanical properties of steel fiber reinforced reactive powder concrete following exposure to high temperature reaching 800 C, *Nucl. Eng. Des.* 241 (7) (2011) 2416–2424.
- [69] M. Noman, M. Yaqub, Restoration of dynamic characteristics of RC T-beams exposed to fire using post fire curing technique, *Eng. Struct.* 249 (2021), 113339.
- [70] F.E. Richart, A. Brandtzaeg, R.L. Brown, Failure of Plain and Spirally Reinforced Concrete in Compression, University of Illinois at Urbana Champaign, College of Engineering, 1929.
- [71] F. He, L. Biolzi, V. Carvelli, Effect of elevated temperature and water re-curing on fracture process of hybrid fiber reinforced concretes, *Eng. Fract. Mech.* (2022), 108885, <https://doi.org/10.1016/j.engfracmech.2022.108885>.
- [72] P.K. Mehta, P.J. Monteiro, *Concrete Microstructure, Properties and Materials*, 2017.
- [73] P.T. Wang, S.P. Shah, A.E. Naaman, Stress-strain curves of normal and lightweight concrete in compression, *J. Proc.* (1978) 603–611.
- [74] S. Popovics, A numerical approach to the complete stress-strain curve of concrete, *Cement Concr. Res.* 3 (5) (1973) 583–599.
- [75] A. Tomaszewicz, Stress-strain Relationship for Concrete, 1984. Report No. STF65A84065.
- [76] W.T. Tsai, Uniaxial compressional stress-strain relation of concrete, *J. Struct. Eng.* 114 (9) (1988) 2133–2136.
- [77] T.H. Wee, M.S. Chin, M.A. Mansur, Stress-strain relationship of high-strength concrete in compression, *J. Mater. Civ. Eng.* 8 (2) (1996) 70–76.
- [78] L.P. Saenz, Discussion of 'Equation for stress-strain curve of concrete, in: P. Desai, S. Krishnan (Eds.), *ACI J. Proc.* 61 (1964) 1229–1235.